Coherent carrier transport and scattering by lattice defects in single- and multibranch carbon nanoribbons

Davide Mencarelli, Tullio Rozzi, and Luca Pierantoni
Dipartimento di Elettromagnetismo e Bioingegneria, Università Politecnica delle Marche, Via Brecce Bianche, 60100 Ancona, Italy
(Received 13 December 2007; revised manuscript received 13 March 2008; published 22 May 2008)

We introduce a theoretical model for the investigation of the scattering properties by defects in semiconducting carbon nanoribbons. The analysis of multichannel coherent transport in the presence of discontinuities is performed by means of a numerical solver, which was previously shown to correctly predict the electronic properties of carbon nanotubes, in some respects analogous to the nanoribbon. A scattering-matrix representation has been used to characterize the propagation and scattering of the periodic wave functions of carriers traveling along the carbon nanoribbon. Results show that reflection of charge is important for the defect types considered, i.e., atomic vacancy, potential deformation, and discontinuity caused by a 120° bifurcation. Reflection may be enhanced by interaction (resonance) between successive or periodic discontinuities. The dependence of scattering on carrier energy, referred to the band edge, has also been investigated: Generally, reflection decreases as carrier energy increases. The analysis suggests that the operation of devices employing carbon nanoribbons, such as nanotransistors, may be quite affected by the presence of lattice defects.

DOI: 10.1103/PhysRevB.77.195435 PACS number(s): 73.22.−f, 72.10.Fk, 05.60.Gg, 03.50.De

I. INTRODUCTION

The analysis of carrier transport in low-dimensional systems[1] is becoming of fundamental importance, as other classes of materials are demonstrated to exist in a stable state. Besides the well known class of one dimensional (1D)-atomic structures, represented by carbon nanotubes (CNTs),[2] emerging freestanding two dimensional (2D) layers of atomic crystal (graphene, single layer boron nitride, and some others[3]) are now attracting great attention as they show promise for material-based electronics and for optoelectronic applications.[4–9]

The scientific relevance of graphene 2D crystal, made of carbon atoms packed in a honeycomb lattice, has already been pointed out in the literature:[3] it features not only very high crystal quality, but it is also so "flexible" as to form the basic constituent of all materials of other dimensionalities, such as zero dimensional fullerenes, 1D nanotubes, or 3D graphite. Ideally, charges are allowed to travel without scattering for thousands of interatomic distances: Electronic mobility is typically very high and transport is nearly ballistic, so that the analogy with a 2D-electron gas in a semiconductor becomes evident. Our analysis is focused on carbon nanoribbon (CNR), as this is an ideal candidate for the building block of future electronics: An example is provided by CNR-FET[10–12] (field effect transistor).

The theoretical gap still existing for a complete characterization of CNRs motivates the need for their accurate modeling. A recent model, previously developed for the analysis of CNTs,[13] is revisited in order to make it suitable for CNRs. Nanoribbons and nanotubes are made of the same hexagonal carbon lattice, and this analogy is evident from their electronic properties.[14–18] Many concepts of CNTs, such as chirality, may be inherited in CNRs: A similar behavior of the dispersion curves follows. As a consequence, CNR can be metallic, semimetallic, or semiconducting, depending on chirality and width.

The use of a multichannel coherent transport model,[1] based on the formalism of transmission line theory, together with an appropriate use of electromagnetic solvers, makes it possible to explain and investigate many aspects of CNR devices. Some interesting examples are provided by the coupling of electronic wave functions with external applied electromagnetic fields, the dependence of charge distribution on geometric parameters and on metal contacts, and charge scattering due to the localized atomic defects, which is the subject of the present work.

Our simulations consider semiconducting CNRs typically 2–3 nm wide, that is, tens of atoms in the transverse section. In the literature, we found just a few contributions to CNR analysis including the fine detail of its periodic lattice: Usually, they consider small structures made of a few carbon atoms in the transverse direction.[10] In cases where large structures are considered, some approximations are exploited, such as tight binding (TB), Dirac, or effective mass formulations: Although accurate in some respects, unfortunately, these formulations imply loss of information about the spatial distribution of the electronic wave functions, which makes them unsuitable to the analysis of CNR discontinuities.

In Sec. I, we present our potential-well model of the carbon lattice and perform a preliminary analysis, taking into exam the case of 2D graphene. Section II is devoted to a detailed explanation of our strategy for the CNR analysis: A scattering-matrix formulation is proposed in order to describe the carrier transport in CNRs, which are seen as periodic electronic waveguides. In Sec. III, we report results and provide an insight on charge scattering due to the lattice defects, which highlights, possibly, real advantages or limitations on the use of CNR devices. We also report an example of multibranch CNR that is likely to appear next, i.e., the counterpart of CNT *Y* junction.[19] Final considerations are made in Sec. V.

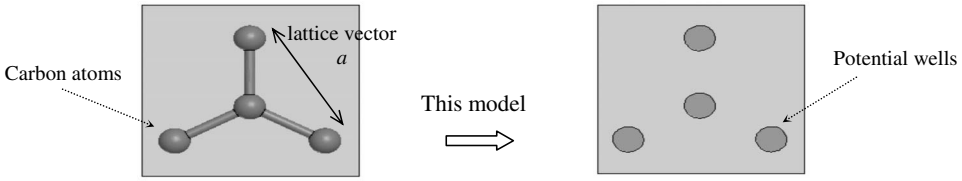

FIG. 1. The "potential well" model of the carbon lattice. The spatial distribution of the potential, i.e., deep and width of the wells, has been set in accordance to Ref. 13.

II. THEORETICAL MODEL

A. Potential-well model of the two-dimesional-carbon lattice

We have previously developed quantum-mechanical models of carbon nanotubes by making use of our home-made Schrödinger-Maxwell Nanowave solver, which exploits the formal analogy between Schrödinger and Maxwell equations in the phasor domain. This point of view allows to exploit the intrinsic flexibility of effective numerical techniques in order to solve problems that have been so far approached by *ad hoc* or simplified models. Moreover, the analysis of the electronic transmission properties of systems characterized by multichannel coherent transport can take advantage of transmission line theory, i.e., a mature technique for the analysis of microwave circuits and devices, which is particularly suited for the analysis of devices of high aspect ratios, possibly loaded by active, periodic, anisotropic, and nonlinear materials.

In the present work, the CNR is modeled as periodic dielectric waveguide or, equivalently, as photonic crystal slab. This kind of approach stems from our mentioned work involving CNTs.[13] In particular, CNTs have been simulated by identifying their carbon atoms with potential wells, which are modeled in the frequency domain by means of dielectric posts. This is shown in Fig. 1, where the lattice vector is also defined: Its length is $3^{1/2}$ times that of the C-C bond[2] ($\sim$1.44 Å). The electric field normal to the plane of the lattice is identified, in our dielectric analogy, with the electronic wave functions.

The Schrödinger equation includes the potential profile $V(x,z)+V_0$, which simulates the following carbon lattice:

$$\nabla^2\Psi = -\frac{2m_0}{\hbar^2}[E + V_0 + V(x,z)]\Psi, \tag{1}$$

where V_0 is the constant potential between the wells, and $V(x,z)$ the additional potential distribution of the periodic wells. The choice of the potential profile is discussed in Ref. 13. Fortunately, it is possible to maintain for the CNR the same model of the CNT. Indeed, this model is even better suited to the CNR problem since this structure does not involve curvature.

B. Dirac formulation of two-dimensional graphene

In the limit of very wide CNRs, the band gap approaches zero and the same happens for the effective mass of charge carriers within the gap valley. This limit can be tested by a straightforward TB approach. As a consequence, the electronic properties of CNR become similar to those of 2D graphene, where, in the neighborhood of the zero-gap points, charge carriers at low energy E may be described as quasiparticles, or Dirac fermions, by the following simple 2D Dirac-like equation:[3]

$$\hbar v_F(\sigma_1\hat{x} + \sigma_2\hat{y}) \cdot \mathbf{k}\Psi = E\Psi, \tag{2}$$

where $\sigma_{1,2}$ are the Pauli matrices, $\mathbf{k}$ is the quasiparticle momentum, and v_F is the Fermi velocity.

Figure 2 shows a comparison between the dispersion curves obtained by TB calculation and by the present formulation, for the case of 2D graphene.[2] The agreement is evident, particularly for carrier energies just above the zero-gap points. Differences appear as a consequence of the full analysis of the periodic potential profile performed here. We note that the Fermi velocity dE/dk at the zero-gap points is about 8×10^5 m/s.

In the present work, the Schrödinger representation (1), rather than the Dirac one, is maintained, as the numerically found wave functions are defined everywhere in the $E(\mathbf{k})$ space and not only just above the zero-gap points. Moreover, we consider "thin" CNRs, a few nm wide, for which band gap and effective mass still have finite values.

III. ANALYSIS OF THE CARBON NANORIBBON

A. Definition of the carbon nanoribbon unit cell and excitation of the nanoribbon

The CNR is considered as an ideal 2D-photonic crystal, finite in the transverse direction, and periodic along its longitudinal axis (z): This allows defining the unit cell of the CNR periodic waveguide, of length L and width W, as shown in Fig. 3(a). In order to perform the simulations, one has to establish the boundary conditions at the sides. In the literature, it is found that the edge effects on CNR dispersion curves are relatively small.[15] In the present work, we will not modify the Hamiltonian in order to account for the different nature of carbon bonds at the edge: Dirichlet conditions have been chosen for the lateral boundary, i.e., $\Psi(0,z)=0$ and $\Psi(W,z)=0$. This choice seems to be reasonable, as, in fact, no lateral electronic tails or tunneling phenomena are considered.

In order to obtain the electronic dispersion curves, we excite the CNR by means of "Floquet modes,"[20] to be defined below, impinging on its transverse section. A discrete scattering-matrix representation[20] in terms of these Floquet modes is used in order to satisfy the Bloch condition, to which we refer here as Floquet condition.

The chosen excitation section of the CNR is that of the side of the thin homogeneous waveguide shown in Fig. 3(a), which is defined by Dirichlet conditions at $x=(0,W)$. The

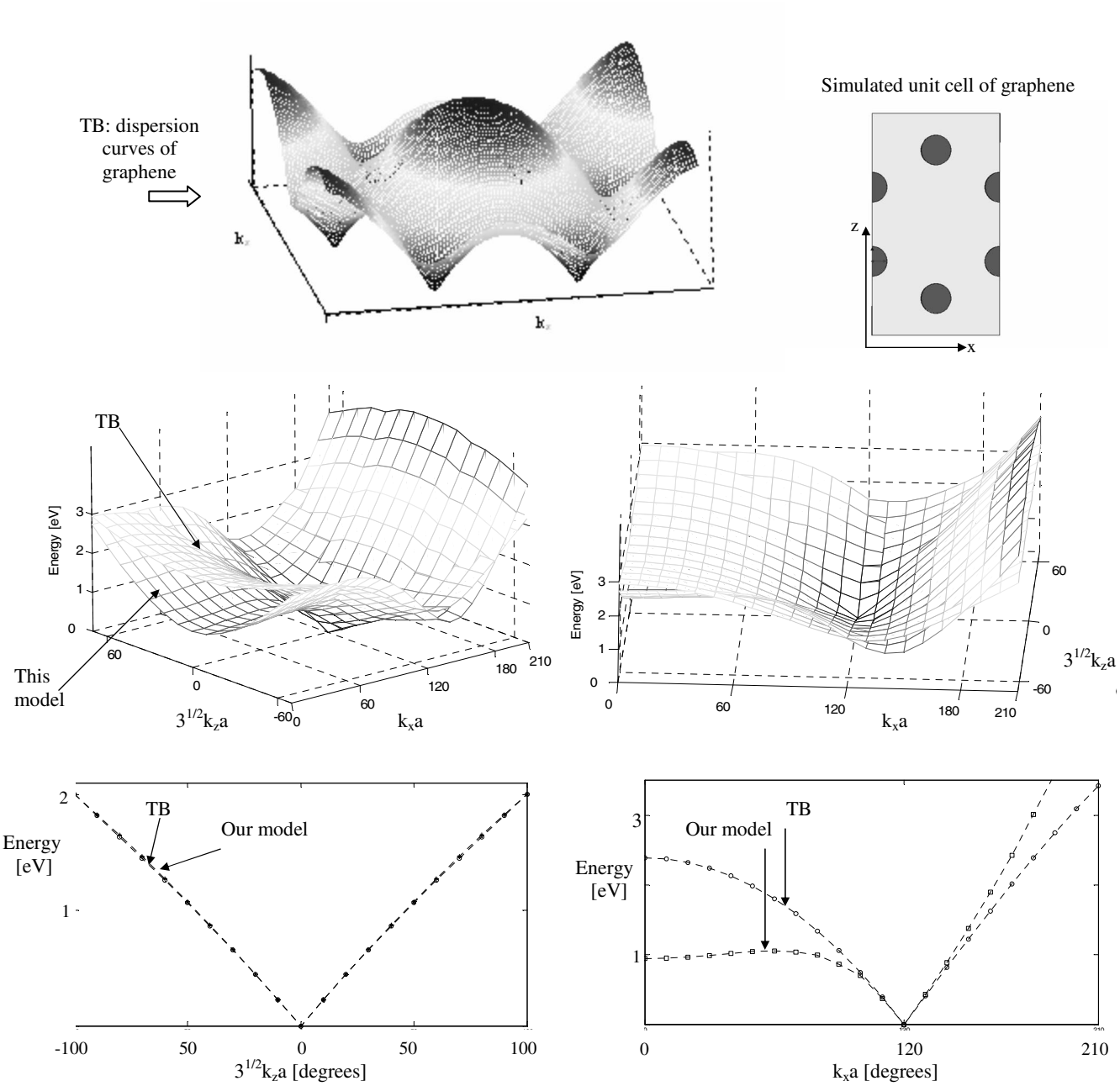

FIG. 2. Graphene dispersion curves: Results obtained by TB and present model are compared for energies above the zero-gap point. The simulated structure, i.e., the unit cell of graphene, is reported. Both 2D-surface and 1D-section comparisons are made.

number of spatial harmonics of the type $\sin(n\pi/W)$ of this waveguide, required to correctly describe the Floquet modes of the CNR, depends only on its width: The larger the CNR, the higher the number of spatial harmonics. The expression Floquet modes refer to the electronic wave functions of the CNR, i.e., linear combinations of the spatial harmonics of the homogeneous waveguide, mixed by the presence of the periodic potential wells, which satisfy the Floquet condition in the z direction and, consequently, the Schrödinger equation. This is, in fact, the harmonic mixing due to the presence of the periodic array of potential wells. It is noted that the problem considered may seem to be 3D: In fact, it is 2D, as the CNR is very thin with respect to the size of the unit cell.

B. Band gap of armchair carbon nanoribbons

As pointed out in many previous papers,[21] the degree of freedom constituted by the spin could be important for zigzag CNRs, where the conduction (bottom) and valence (top) bands are mainly composed of edge states. However, it can be disregarded for armchair CNRs, which have been analyzed in the present work.

CNRs with armchair shape edges on both sides are classified by the number of dimer lines N_a across the ribbon width.[22] Following the same line of reasoning of Ref. 15, the TB calculation can be corrected in order to account for the hydrogen bonds at the edges: The main change follows from the modification of the site energy, due to the difference be-

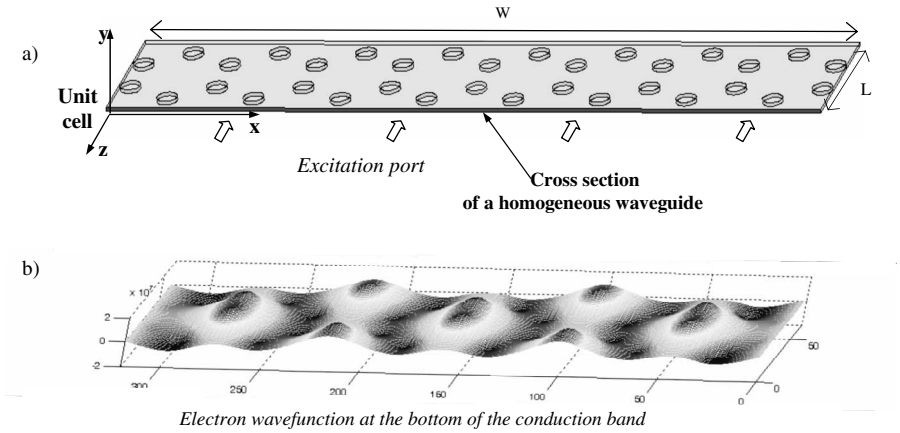

FIG. 3. (a) Side excitation of the CNR (only the unit cell is shown). (b) Example of simulated electronic wave function. Dirichlet conditions impose vanishing of the wave function at the side boundary.

tween the carbon and hydrogen electronegativities. A choice of the site energy=bulk energy+0.3t, where t is the "transfer energy" (~ -3 eV), leads to a relatively small change of the band gap, which is less than 10% for CNRs whose size is in the range considered here, see Fig. 4. Moreover, the inversion symmetry is broken and the Fermi energy is offset from the zero bulk energy.

Other works,[22,23] based on more rigorous first principles calculations, show that the actual dispersion curves of armchair CNRs differ from those obtained by TB model, in the following ways:

(1) The hierarchy of the gap size Δ passes from $\Delta_{(\mathrm{Na}=3p)} > \Delta_{(\mathrm{Na}=3p+1)} > \Delta_{(\mathrm{Na}=3p+2)}$ to $\Delta_{(\mathrm{Na}=3p+1)} > \Delta_{(\mathrm{Na}=3p)} > \Delta_{(\mathrm{Na}=3p+2)}$, where p is an integer.

(2) A small gap rises also for CNR of the type $(3p+2)$.

Moreover, the difference from TB results observed in Refs. 22 and 23 is a little stronger than that reported in Fig. 4, which is obtained following Ref. 15. The model of Refs. 22 and 23 and the model of Ref. 15 point, qualitatively, to the same direction for what concern the difference (2) but to the opposite direction with regard to the difference (1), as, in fact, the hierarchy of the gap size does not change in the curves of Fig. 4. In any case, both models show that corrections tend to decrease with CNR width and are fairly small for CNRs as wide as those considered in this work.

In Table I, we report the gap obtained with the mentioned different approaches, respectively, TB, TB corrected as in Ref. 15, model of Ref. 23, and our method. Data are relative to three CNRs of the polyperylene series,[15] corresponding to $(3p)$, $(3p+2)$, and $(3p+1)$ types, with $p=5$, $p=5$, and $p=6$, respectively. Despite the non-negligible difference between the above models, band gap results show a substantial agreement in the range of CNR widths considered in the present work.

C. Scattering matrix

The direct excitation of the CNR by its electronic wave functions gives us the unique opportunity to analyze the effect on charge transport of discontinuities, local potential changes, lattice defects, bending, graft of new branches, change of lattice orientation, etc. The local potential energy seen by electrons (holes) traveling along the CNR can be varied in order to locate the carrier in an arbitrary position above the bottom (below the top) of the conduction (valence) band. This is done by simply adjusting the potential profile in the model so as to represent the incremental energy. In this way, the numerical simulations give an insight on the dependence on energy of all the above phenomena (propagation, reflection, and scattering).

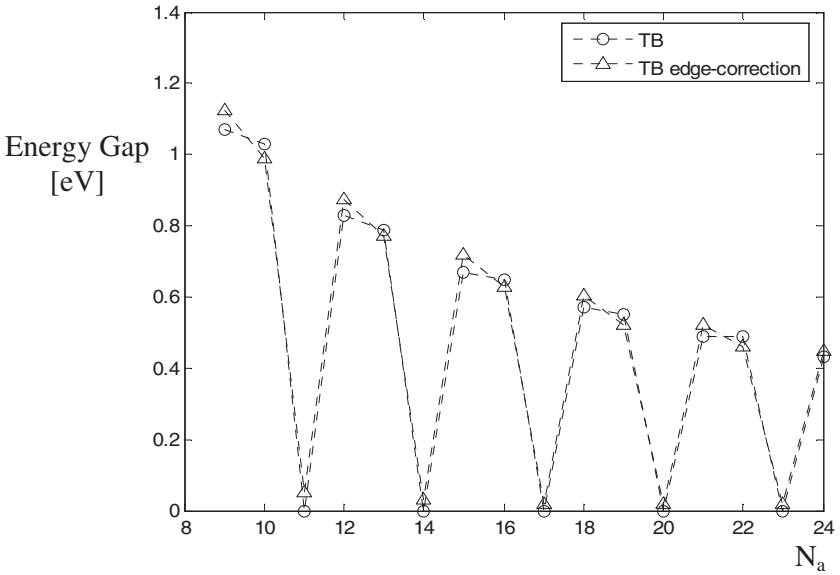

FIG. 4. Comparison between band gaps of armchair CNRs calculated by TB approach and by TB with edge correction: curves are plotted as function of N_a.

TABLE I. CNR gap obtained with four different approaches.

N_a	TB (eV)	TB edge correction as in Ref. 15 (eV)	Model of Ref. 23 (eV)	Our model (eV)
15	0.67	0.72	0.49	0.65
17	0	0.02	0.11	0.09
19	0.55	0.52	0.6	0.5

Moreover, this approach fits very well the features of nano-FET devices,[10–12] where carrier energy is controlled and continuously varied by means of a "gate" electrode. In nano-FETs, the channel conductivity is controlled by varying the probability of charge tunneling: Lattice defects and discontinuities along the channel are expected to strongly affect the device operation and performance. In the following, we show the derivation of the scattering matrix $\hat{\mathbf{S}}$ of an arbitrary length of CNR containing a discontinuity. A brief summary is provided in Fig. 5. Let us chose an energy level for an electron traveling just above the conduction band edge. It was stated before that an adequate number of spatial harmonics, say, N, of the homogeneous waveguide, whose cross section is shown in Fig. 3, is required in order to describe the Floquet modes of the CNR, i.e., to account for the mixing of harmonics due to the potential wells. An important point to be highlighted is that, even though N may actually be relatively small, we may need to excite the unit cell with many more harmonics, two times N or more, in order to ensure that any residual coupling between harmonics is accounted for. This operation has to be carried out at least once as a preprocessing step.

The excitation set fixed by the choice of N is then used also in order to characterize a finite piece of CNR made of an arbitrary (compatibly with the computational cost) number of unit cells and containing defects. The whole structure is simulated as a two-port network: 2 is the number of physical ports, and $2N$ that of virtual and actual ports. The solution of the eigenvalue problem arising from the Floquet condition applied to the unit cell yields, at any chosen energy, the new model basis of Floquet modes, which we use as "reference system" for any further computation.

Indicating by S^u the scattering matrix of the unit cell in the representation of the spatial harmonics, and by $\mathbf{a}$, $\mathbf{b}$ the incident and reflected traveling-wave amplitudes of the harmonics, we have

$$\begin{bmatrix} \mathbf{b_1} \\ \mathbf{b_2} \end{bmatrix} = \mathbf{S}^u \begin{bmatrix} \mathbf{a_1} \\ \mathbf{a_2} \end{bmatrix} = \begin{bmatrix} \mathbf{S}^u_{11} & \mathbf{S}^u_{12} \\ \mathbf{S}^u_{12} & \mathbf{S}^u_{22} \end{bmatrix} \begin{bmatrix} \mathbf{a_1} \\ \mathbf{a_2} \end{bmatrix}, \tag{3}$$

where

$$\mathbf{b_1} = (b_{1,1}, b_{1,2} \ldots b_{1,N}), \quad \mathbf{b_2} = (b_{2,1}, b_{2,2} \ldots b_{2,N}),$$

$$\mathbf{a_1} = (a_{1,1}, a_{1,2} \ldots a_{1,N}), \quad \mathbf{a_2} = (a_{2,1}, a_{2,2} \ldots a_{2N}).$$

The charge wave function at the beginning of the unit cell, with reference to Fig. 3, is given by

$$\Psi(x, z=0) = \sum_{1 \le n \le N} \left[a_{1,n} e^{-ik_n z} \frac{1}{\sqrt{k_n}} \sin\left(\frac{n\pi}{W} x\right) + b_{1,n} e^{ik_n z} \frac{1}{\sqrt{k_n}} \sin\left(\frac{n\pi}{W} x\right) \right]_{z=0}, \tag{4}$$

where the factor $1/\sqrt{k_n}$ is used to normalize the scattering parameters, n is an integer, and

$$k_n = \sqrt{\frac{2m_0}{\hbar^2}(E + V_0) - (n\pi/W)^2} \quad \text{if } n\pi/W > \sqrt{E + V_0}$$

or

$$k_n = -i\sqrt{\frac{2m_0}{\hbar^2}(E + V_0) - (n\pi/W)^2} \quad \text{otherwise.}$$

Before imposing its periodic condition, Eq. (3) is linearly transformed as follows:

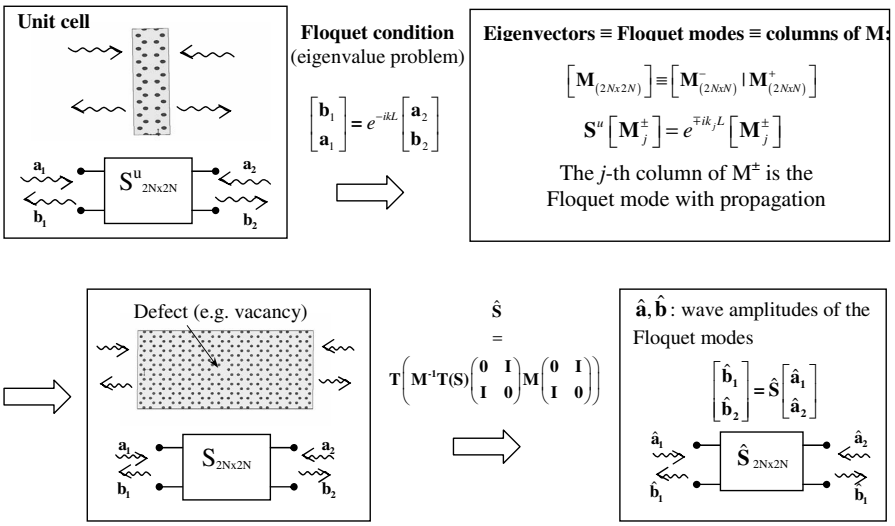

FIG. 5. Steps needed to obtain the scattering matrix $\hat{\mathbf{S}}$ of a CNR containing a discontinuity, in terms of Floquet modes.

$$\begin{bmatrix} \mathbf{b}_1 \\ \mathbf{a}_1 \end{bmatrix} = \mathbf{T}(\mathbf{S}^u) \begin{pmatrix} \mathbf{0} & \mathbf{I} \\ \mathbf{I} & \mathbf{0} \end{pmatrix} \begin{bmatrix} \mathbf{a}_2 \\ \mathbf{b}_2 \end{bmatrix}, \tag{5}$$

where $\mathbf{I}$ $(N \times N)$ is the identity matrix and

$$\mathbf{T}(\mathbf{X}) = \mathbf{T}\left(\begin{bmatrix} \mathbf{X}_{11} & \mathbf{X}_{12} \\ \mathbf{X}_{21} & \mathbf{X}_{22} \end{bmatrix} \right) = \begin{bmatrix} -\mathbf{X}_{12}^{-1}\mathbf{X}_{11} & \mathbf{X}_{12}^{-1} \\ \mathbf{X}_{21}^{u} - \mathbf{X}_{22}\mathbf{X}_{12}^{-1}\mathbf{X}_{11} & \mathbf{X}_{22}\mathbf{X}_{12}^{-1} \end{bmatrix} \quad \mathbf{T}(\mathbf{T}(\mathbf{X})) = \mathbf{X}. \tag{6}$$

Imposing the Floquet condition means

$$\begin{bmatrix} \mathbf{b}_1 \\ \mathbf{a}_1 \end{bmatrix} = \mathbf{T}(\mathbf{S}^u) \begin{pmatrix} \mathbf{0} & \mathbf{I} \\ \mathbf{I} & \mathbf{0} \end{pmatrix} \begin{bmatrix} \mathbf{a}_2 \\ \mathbf{b}_2 \end{bmatrix} = e^{-ikL} \begin{bmatrix} \mathbf{a}_2 \\ \mathbf{b}_2 \end{bmatrix}, \tag{7}$$

so that the Floquet modes are found from the solution of the following eigenvalue problem:

$$\left[\mathbf{T}(\mathbf{S}^u) \begin{pmatrix} \mathbf{0} & \mathbf{I} \\ \mathbf{I} & \mathbf{0} \end{pmatrix} - e^{-ik_j L} \right] \cdot \mathbf{M}_j = 0$$

For example, Eq. (4) for the jth Floquet mode becomes

$$\Psi_j(x, z=0) = \sum_{1 \le n \le N} \left[(M_{n,j} + M_{n+N,j}) \frac{1}{\sqrt{k_n}} \sin\left(\frac{n\pi}{W} x \right) \right], \tag{8}$$

where the columns of the matrix $\mathbf{M}$ are the eigenvectors.

Indicating with $\mathbf{S}$ the scattering matrix of a finite piece of CNR containing the following localized defect:

$$\begin{bmatrix} \mathbf{b}_1 \\ \mathbf{b}_2 \end{bmatrix} = \mathbf{S} \begin{bmatrix} \mathbf{a}_1 \\ \mathbf{a}_2 \end{bmatrix}, \tag{9}$$

it is possible to derive the new scattering matrix $\hat{\mathbf{S}}$, referred to the Floquet basis, as

$$\hat{\mathbf{S}} = \mathbf{T}\left[\mathbf{M}^{-1}\mathbf{T}(\mathbf{S}) \begin{pmatrix} \mathbf{0} & \mathbf{I} \\ \mathbf{I} & \mathbf{0} \end{pmatrix} \mathbf{M} \begin{pmatrix} \mathbf{0} & \mathbf{I} \\ \mathbf{I} & \mathbf{0} \end{pmatrix} \right],$$

$$\begin{bmatrix} \hat{\mathbf{b}}_1 \\ \hat{\mathbf{b}}_2 \end{bmatrix} = \hat{\mathbf{S}} \begin{bmatrix} \hat{\mathbf{a}}_1 \\ \hat{\mathbf{a}}_2 \end{bmatrix}, \tag{10}$$

where $\hat{\mathbf{a}}$ and $\hat{\mathbf{b}}$ are the vectors of amplitudes of the Floquet modes.

IV. RESULTS

A. Nanoribbon discontinuities

In the present work, we are dealing with three different types of CNR discontinuities: (a) vacancy defect, which is simulated by removing one of the potential wells of the CNR; (b) local potential deformation, which we mimic by varying the diameter of a potential well; (c) Y junction, that is, the 120° bifurcation. Our model provides a direct way to analyze the effects of localized lattice defects, i.e., (1) the amplitude and phase of transmission and/or reflection coefficients of electronic wave functions (Floquet modes); (2) the mutual coupling between wave functions of any bands or subbands.

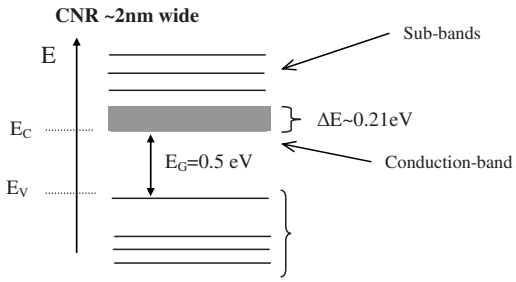

FIG. 6. E_c and E_v are the conduction and valence band energies, respectively.

The analysis is performed under the most general condition, i.e., the multiband situation. However, since the energy range ΔE under study, shown in Fig. 6, is chosen such that only the fundamental band is propagating (above cutoff), just item 1 referred to the same band is really significant. Floquet modes that correspond to carriers belonging to the subbands are below cutoff and rapidly attenuate as they propagate.

It is observed that the $\mathbf{S}_{2N\times 2N}^{u}$ matrix of the unit cell is typically made of distinct blocks corresponding to distinct and noninteracting groups of spatial harmonics. As a consequence, the analysis of the effect of a CNR discontinuity, for example, on the propagating Floquet mode, can be simplified just by considering the appropriate subblock of the $\mathbf{S}$ matrix (9), which involves a number $N' < N$ of harmonics.

Alternatively, it is possible to excite the structure directly containing the discontinuity by only the N' harmonics above: In this case, the advantage of a simpler excitation is offset by the necessity of placing the excitation ports far away from the discontinuity and, consequently, of increasing the computational domain, in order to make the attenuated Floquet modes inaccessible, which are not well described by only N' harmonics. The best choice depends of many factors, including, in particular, the nature of the discontinuity, which may bring about more or less coupling between modes, and the features of the solver used, for example, the supported aspect ratio and possible limitations to the maximum number of allowed harmonics.

B. Numerical test: Unperturbed nanoribbon

Although an experimental validation is not currently available, our results are believed to be quantitatively reliable as the model was previously tested by comparing the dispersion curves of CNTs of different chiralities, for energy values around the band gap, with TB results, and by including challenging complications, such as band distortion due to a strong applied electric field and metal contacts.

Before proceeding with our main results, a simple test was carried out in order to demonstrate numerical self-consistency. It is actually not trivial to verify that, for a relatively long piece of unperturbed CNR, carriers are not reflected, as instead it may be expected from cumulative loss of accuracy of the solver and from truncation of the number of harmonics N to a finite value.

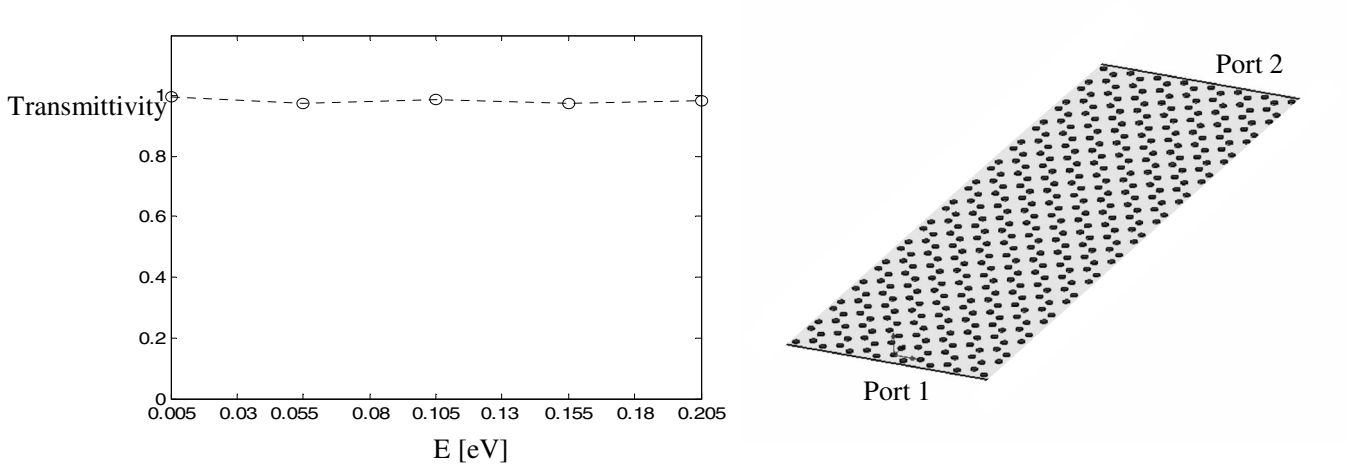

FIG. 7. Numerical test: simulation of a length of CNR, formed by 14 unit cells. The transmittivity is nearly unity over the whole energy range analyzed.

In fact, Fig. 7 shows that the transmission probability (amplitude square) from "Port 1" to "Port 2" of a CNR with $N_a=15$ is nearly unity over the whole energy range considered (this range refers to the bottom of the conduction band, as shown in Fig. 6). The numerical self-consistency of the approach is then confirmed.

C. Examples

In the following, the scattering properties of the aforementioned three types of discontinuities are reported.

Figure 8 shows the transmittivity of the electrons traveling across a defect formed by an atomic vacancy. The zero energy corresponds to the bottom of the conduction band: As expected, at this point, transmission abruptly drops; on the contrary, i.e., for carriers traveling at the higher energies, the discontinuity is shown to have a weaker effect on the scattering of the wave function. This also seems quite reasonable.

A similar energy dependence is found, in Fig. 9, for a defect modeled as a modified potential well, i.e., a potential well with an increased radius. Figure 9 shows, in addition, the dependence of the transmittivity on the defect radius for a fixed carrier energy.

Figure 10 shows a Y junction, with 120° rotational symmetry: This choice preserves the structure of the lattice without deformation, since the same angle is formed by the sides of the carbon hexagons. In this case, we report the fraction of reflected charge at the discontinuity.

In general, we observe that carriers experience a nonnegligible reflection, at least 10% (amplitude square), even for small discontinuities. This is not surprising if we consider that the CNR is a periodic waveguide for carrier transport, where propagation takes place through constructive interference between the plane waves scattered by carbon atoms, so that even a small break of the lattice periodicity produces a considerable effect. In fact, experimental evidence shows that missing carbon atoms in the crystal lattice cause strong scattering.[24] These effects may become critical in the fabrication of real CNR devices, where particular care ought to be taken of the crystal quality, as it may strongly impact on device performance. It is noted, however, that the currently

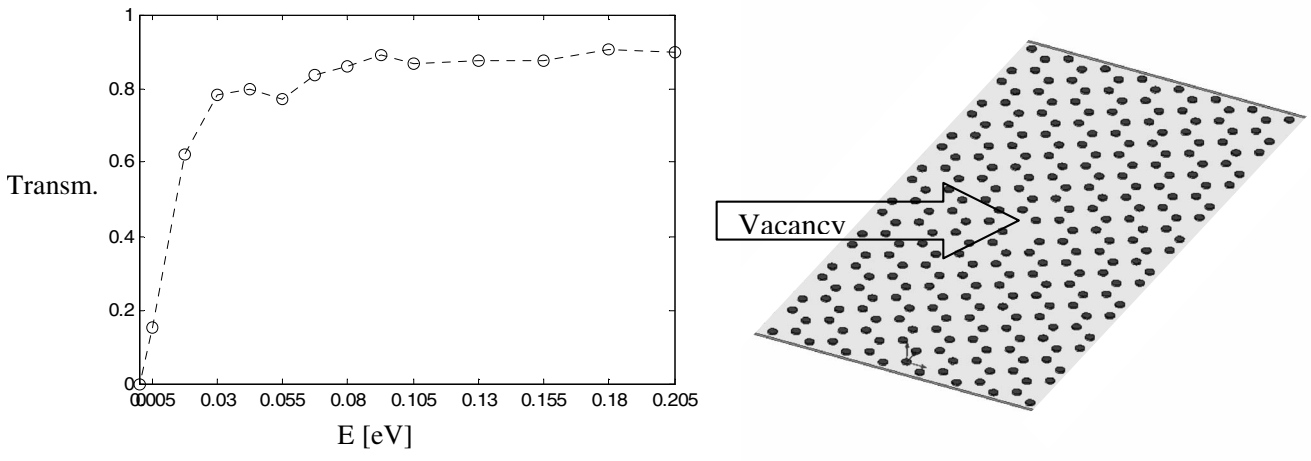

FIG. 8. Transmittivity through a vacancy defect, as function of the electron energy.

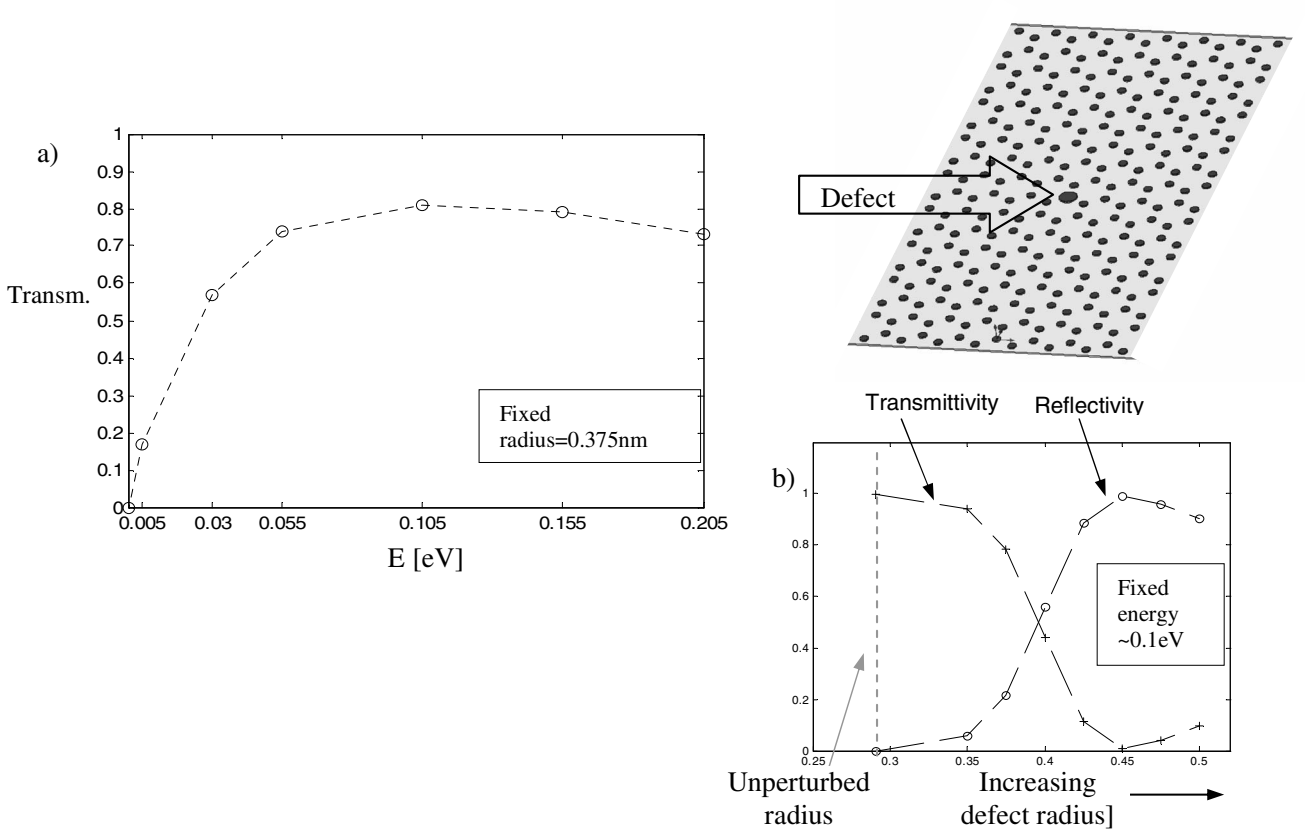

FIG. 9. Transmittivity through a local potential deformation, as function of the (a) electron energy and (b) defect radius.

obtainable CNRs, wider than 10–15 nm, ought to be less sensitive to single localized defects. As an example, considering a vacancy in a CNR of half of the simulated width W, the transmittivity of carriers with a 0.2 eV energy reduces from 90% to less than 40%.

Finally, it is noted that the present approach can be applied to very long and complex structures containing localized defects or discontinuities: Each unperturbed length of CNR is simply represented by the matrix $\hat{\mathbf{S}}$ of a cascade of unit cells and any discontinuity can be characterized as described above. The scattering parameters of the whole structure follow from the cascade of the scattering matrices of its substructures. An interesting example is given by the interference effects caused by a pair of cascaded vacancies located along the longitudinal symmetry axis of the CNR: Fig. 11 shows the transmission probability of electrons through the vacancies as a function of their distance D and of the carrier energy. Maxima and minima correspond to the constructive and destructive interferences: They are spaced by a quarter of carrier wavelength. As expected, at higher energies, the wavelength decreases, the standing wave ratio decreases, and carriers experience an increased transmittivity.

It is noted that the cooperating effect of two vacancies may produce complete electronic transmission or, on the other hand, it may strongly emphasize the wave function reflection.

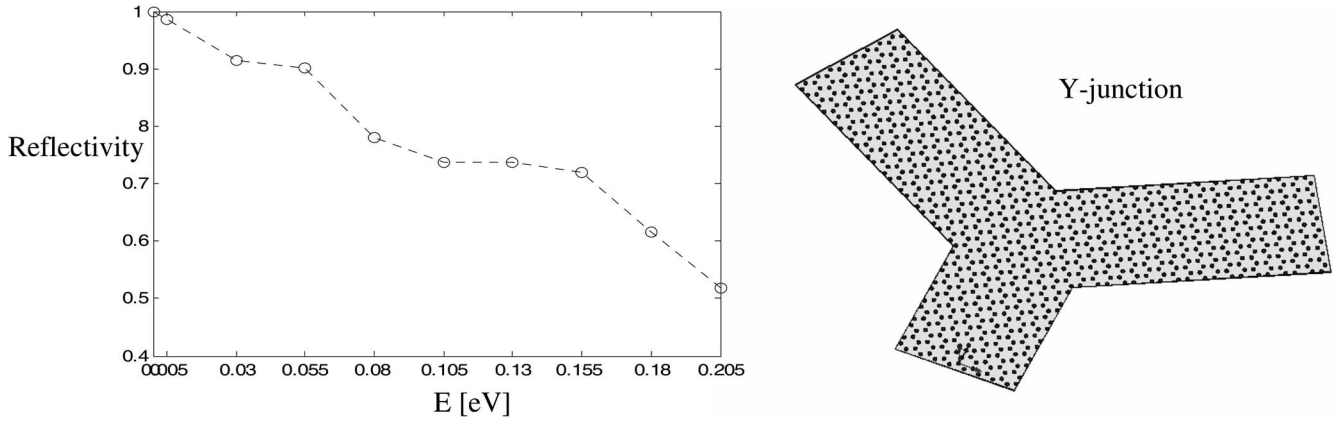

FIG. 10. Reflectivity of a 120° bifurcation, as function of the electron energy.

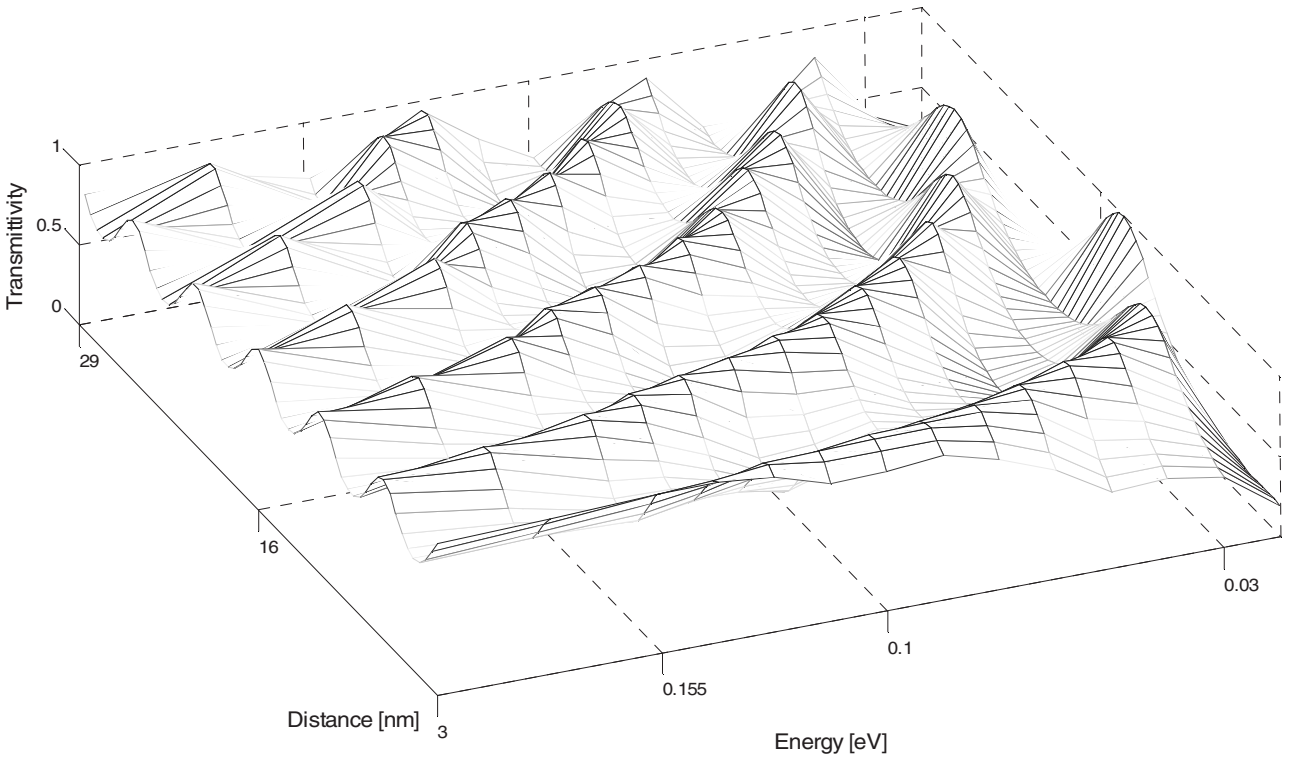

FIG. 11. Transmittivity through a pair of vacancies positioned along the CNR axis. The surface is plotted with respect to the carrier energy and distance between vacancies.

Table II reports the reflectivity of vacancy defects offset in the x direction from the symmetry axis of the CNR, for two values of carrier energy. The reflection is generally higher for vacancies placed along the CNR axis. As shown in the table, the offsets from the axis are taken as multiples of the lattice vector a.

In Fig. 12, we report the transmittivity through a pair of cascaded vacancy defects, as a function of θ, which is the phase retardation of the propagating Floquet mode in traveling between the two vacancies. The sharper curve corresponds to the case of vacancies placed along the CNR axis; the other curve is obtained by placing one of the two vacancies a distance a from the axis. In the latter case, the resulting "resonant cavity" is not symmetric and its resonance cannot provide complete carrier transmission.

D. Periodic impurities in carbon nanoribbons

In this section, we include the results about periodic defects in armchair CNRs. In this way, we provide an example of the expected behavior of charge transport in CNR with a given concentration of substitutional impurities, showing the transport dependence on the strength of the impurity potential. As already described above, the analysis is carried out by employing an idealized impurity, which is simulated by means of an increased area of the corresponding potential well.

TABLE II. Reflectivity of vacancy defects offset in the x direction from the symmetry axis of the CNR for two values of carrier energy.

Offset	0	a	$2a$	$3a$
Reflectivity (E=0.205 eV)	0.091	0.019	0.048	0.083
Reflectivity (E=0.055 eV)	0.248	0.021	0.156	0.128

The presence of impurities is shown to affect the unperturbed dispersion curves in that they open new band gaps, whose width increases with the strength of the perturbing defects expressed by the area of their potential well. The new band gaps are associated with forbidden energy levels for carrier propagation, or, considering a finite length of CNR, to strong dips of transmission.

In Fig. 13, we compare the dispersion relation of an unperturbed CNR (N_a=19) to that of a perturbed CNR (N_a =19): The latter is described by a supercell with 266 carbon atoms containing a substitutional impurity at its center, which corresponds to having a defect concentration of ~0.38%. Energies lie, as usual, just above the bottom of the conduction band. We consider three different values of the defect size, showing how strongly this affects the width of the opening band gaps. As expected, resonances are centered at energies corresponding to $k(E)L_s=n\pi$, where L_s is the length of the supercell and n is an integer: This "electronic" Bragg condition implies that the interference of wave functions, due to the periodic defects, constructively acts, in such a way that the carrier reflection along the CNR is maximized. As pointed in Ref. 25, the substitutional atoms act as scattering centers for the electronic transport along the nanoribbons, reducing the transmittance channels. This produces a

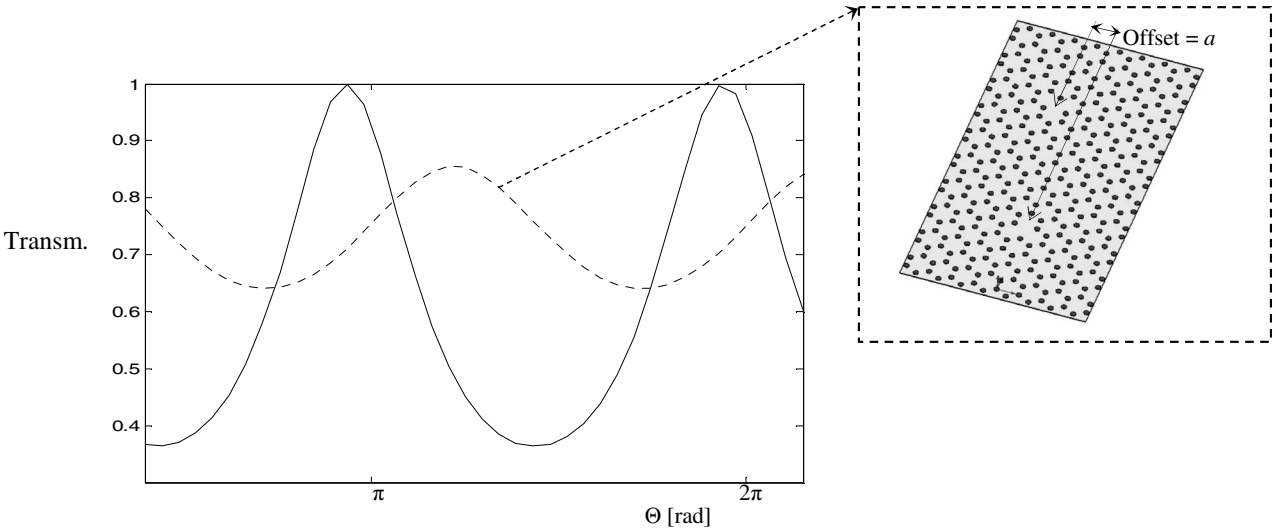

FIG. 12. Transmission probability for carriers of energy 0.055 eV through a pair of vacancy defects, as a function of the phase retardation $\theta=kD$ of the propagating Floquet mode. The solid curve results from two vacancies along the CNR axis, and the dashed one is obtained with one of the two vacancy offsets from the axis by a, as shown in the inset.

reduction of the free mean path for carriers, analogous to the drop of mobility in doped CNTs.[26]

V. CONCLUSION

We have discussed the effects of discontinuities on carrier propagation in carbon nanoribbons, for different types of lattice defects. We provide an estimation of the scattering properties of electron wave functions, i.e., reflectivity and transmittivity, and quantify their dependence on carrier energy. Results suggest that, due to the resonant nature of the carrier propagation in the periodic waveguide formed by the CNR, even small defects can produce appreciable reflection.

Our analysis enables the investigation of the operation of CNR-FETs under the realistic condition of imperfect channel transport. Additionally, we analyze a Y junction, which may be an important example of a multibranch circuit, realized on the nanonoscale, for electronic devices of future generation. As an example of the potential utility of the presented model, we also investigate the scattering properties of both periodic and aperiodic cascaded defects, where "resonant" behavior may occur under some conditions.

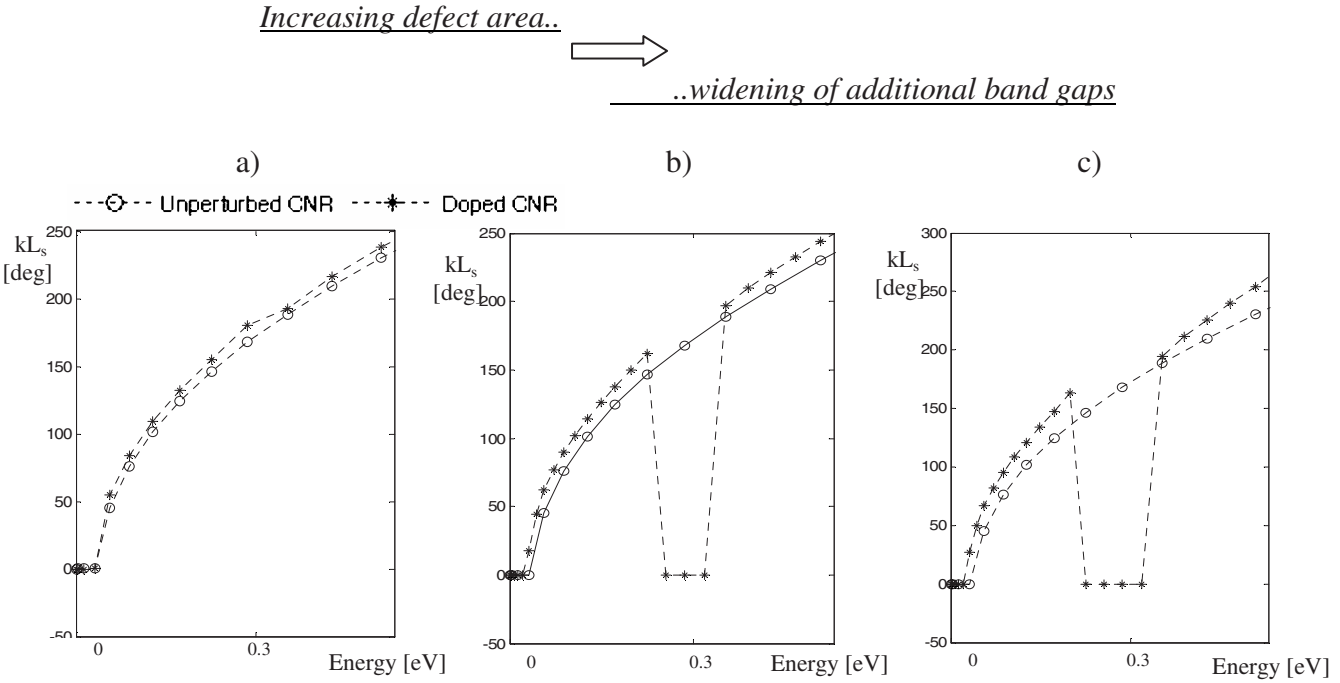

FIG. 13. Comparison between conduction band profiles (energy is referred to the band bottom) of unperturbed CNR and periodically modified CNR (defect concentration of ~0.38%). (a)–(c) report the comparison for a defect radius of 3.2, 3.4, and 3.6 Å, respectively.

[1] J. H. Davies, *The Physics of Low-Dimensional Semiconductors* (Cambridge University, Cambridge, 1998).
[2] R. Saito, G. Dresselhaus, and M. S. Dresselhaus, *Physical Properties of Carbon Nanotubes* (Imperial College, London, 1998).
[3] M. L. Katsnelson, Mater. Today **10**, 20 (2007).
[4] M. Freitag, J. Chen, J. Tersoff, J. C. Tsang, Q. Fu, J. Liu, and P. Avouris, Phys. Rev. Lett. **93**, 076803 (2004).
[5] J. Ung Lee, Appl. Phys. Lett. **87**, 073101 (2005).
[6] M. Freitag, Y. Martin, J. A. Misewich, R. Martel, and P. Avouris, Nano Lett. **3**, 1067 (2003).
[7] K. Balasubramanian, Y. Fan, M. Burghard, R. Martel, K. Kern, M. Friedrich, U. Wannek, and A. Mews, Appl. Phys. Lett. **84**, 2400 (2004).
[8] X. Qiu, M. Freitag, V. Perebeinos, and P. Avouris, Nano Lett. **5**, 749 (2005).
[9] D. L. John, L. C. Castro, P. J. S. Pereira, and D. L. Pulfrey, Nanotechnology **3**, 65 (2004).
[10] Y. Ouyang, Y. Yoon, and J. Guo, IEEE Trans. Electron Devices **54**, 2223 (2007).
[11] G. Liang, N. Neophytou, D. E. Niconov, and M. S. Lundstrom, IEEE Trans. Electron Devices **54**, 677 (2007).
[12] B. Obradovic, R. Kotlyar, F. Heinz, P. Matagne, T. Rakshit, M. D. Giles, and M. A. Stettler, Appl. Phys. Lett. **88**, 142102 (2006).
[13] D. Mencarelli T. Rozzi, L. Maccari, A. DiDonato, and M. Farina, Phys. Rev. B **75**, 085402 (2007).
[14] M. Y. Han, B. Özyilmaz, Y. Zhang, and P. Kim, Phys. Rev. Lett. **98**, 206805 (2007).
[15] M. Ezawa, Phys. Rev. B **73**, 045432 (2006).
[16] V. Barone, O. Hod, and G. E. Scuseria, Nano Lett. **6**, 2748 (2006).
[17] P. Kim, T. W. Odom, J.-L. Huang, and C. M. Lieber, Phys. Rev. Lett. **82**, 1225 (1999).
[18] H. S. Gokturk, Proceedings of the 5th Conference on Nanotechnology, Nagoya, Japan, July 2005, Vol. 2, pp. 677–680.
[19] A. N. Andriotis, M. Menon, D. Srivastava, and L. Chernozatonskii, Phys. Rev. Lett. **87**, 066802 (2001).
[20] R. E. Collin, *Field Theory of Guided Waves* (IEEE, New York, 1991).
[21] L. Yang, C. H. Park, Y.-W. Son, M. L. Cohen, and S. G. Louie, Phys. Rev. Lett. **99**, 186801 (2007).
[22] Y.-W. Son, M. L. Cohen, and S. G. Louie, Phys. Rev. Lett. **97**, 216803 (2006).
[23] X. Li, X. Wang, L. Zhang, S. Lee, and H. Dai, Science **319**, 1229 (2008).
[24] Engineering & Technology (IET) **2**, 47 (2007).
[25] T. B. Martins, R. H. Miwa, A. J. R. da Silva, and A. Fazzio, Phys. Rev. Lett. **98**, 196803 (2007).
[26] J.-C. Charlier, X. Blase, and S. Roche, Rev. Mod. Phys. **79**, 677 (2007).